IEEE Access
Multidisciplinary | Rapid Review | Open Access Journal

Received 21 November 2025, accepted 9 December 2025, date of publication 5 January 2026, date of current version 8 January 2026.

Digital Object Identifier 10.1109/ACCESS.2025.3650600

RESEARCH ARTICLE

Performance Adoption of an Integrated S-Shaped Double Stator Generator With MPPT and BMS for Renewable Applications

NUR AMIRA IBRAHIM[1], NORHISAM MISRON[1,2,3], (Member, IEEE), HAIRUL FAIZI HAIRULNIZAM[1], ADAM ADZRIN SYAH[1], AND CHOCKALINGAM ARAVIND VAITHILINGAM[4,5], (Senior Member, IEEE)

[1]Faculty of Engineering, Universiti Putra Malaysia, Serdang, Selangor 43400, Malaysia
[2]Institute of Nanoscience and Nanotechnology, Universiti Putra Malaysia, Serdang, Selangor 43400, Malaysia
[3]Institute of Plantation Studies, Universiti Putra Malaysia, Serdang, Selangor 43400, Malaysia
[4]Clean Technology Impact Laboratory, Taylor's University, Subang Jaya, Selangor 47500, Malaysia
[5]Vel Tech Rangarajan Dr. Sangunthala R and D Institute of Science and Technology, Chennai, Tamilnadu 600062, India

Corresponding author: Norhisam Misron (norhisam@upm.edu.my)

ABSTRACT The growing demand for compact and reliable renewable energy systems has intensified research into Permanent Magnet Synchronous Generators (PMSGs) for low-speed applications. This study presents the integration and experimental validation of an S-shaped Interior Embedded Double Stator Generator (S-shaped IEDSG) combined with a Maximum Power Point Tracking (MPPT) controller and a Battery Management System (BMS). A comparative experimental investigation was conducted using three coil configurations, namely inner stator, outer stator, and double stator, to evaluate their charging thresholds, current outputs, and charging durations under different operating speeds. The inner stator produced the highest peak charging power of 263 W but required a higher operating speed of 650 rpm to begin charging. The outer stator started charging at a lower speed of 150 rpm but exhibited lower current and longer charging time exceeding 500 minutes. The double stator configuration demonstrated balanced performance by combining early charging initiation, sustained high power output of about 250 W, and shorter total charging time of less than 400 minutes. These findings confirm that integrating the S-shaped IEDSG with the MPPT controller and BMS enhances charging performance and stability, establishing its potential as a compact and reliable solution for small-scale renewable energy systems such as pico-hydro and wind power generation.

INDEX TERMS AC voltage, charging current, charging power, charging rate, charging voltage, double stator generator, electrical power, PMSM.

I. INTRODUCTION

Permanent Magnet Synchronous Machines (PMSMs) are increasingly adopted worldwide due to rising energy demand, expanding electrification, and the global effort to mitigate climate change. Permanent Magnet Synchronous Generators (PMSGs) are particularly attractive for renewable energy systems because of their compact construction and ability to operate in direct-drive configurations that eliminate mechanical gear losses [1], [2], [3], [4]. Gearboxes are often associated with mechanical losses, noise, and frequent maintenance, making direct-drive PMSGs an appealing alternative for reliable, low-maintenance power generation.

Recent developments in PMSG technology have focused on improving structural design to enhance energy conversion performance. Major innovations include double-rotor configurations [5], [6], as well as single stator [7], [8] and double stator topologies [9], [10], [11], [12], [13], [14], each compatible with either surface-mounted permanent magnets (SPMs) or interior permanent magnets (IPMs).

The associate editor coordinating the review of this manuscript and approving it for publication was Simone Minucci.

The single-stator PMSG remains the most widely adopted design; however, it typically requires many slots and poles to achieve high output power, increasing size and cost. In contrast, the double-stator architecture offers better space utilization within the rotor and reduces magnetic-flux leakage through the shaft [15].

Previous studies have reported that double-stator PMSMs exhibit higher torque and power density compared to single-stator machines [16]. In electric-vehicle systems, interleaved double-stator configurations have been shown to lower vibration and volume by integrating grid inductances [17]. Similar advantages have been demonstrated for compact direct-drive generators [18]. which can also provide redundant or auxiliary power channels for enhanced system reliability [19].

Although SPM machines are simpler to construct, their weak armature reaction and low inductance limit field-weakening capability and torque production [7], [8]. IPM machines, with magnets embedded in rotor laminations, offer stronger magnetic coupling and superior mechanical strength, resulting in higher torque density and better magnet utilization.

These characteristics make IPM generators well suited for renewable energy systems such as hydro and wind turbines [20], [21], where low-speed, high-torque operation is often required. Similarly for hydro turbines, particularly small-scale or pico-hydro systems intended for rural electrification, this generator compactness, high efficiency, and robustness are critical to minimizing system complexity while maximizing energy output [22]. With variable-speed conditions such as wind energy generators deliver high power density and maintaining efficient energy conversion across a wide speed range [23]. Chen et al. [24] compared SPM and IPM generators for direct-drive wind systems and reported that IPMs achieve 5 % higher torque density, 1.5 times lower magnet losses, and 9 % lower copper losses. Roshanfekr et al. [25] further showed that an IPM wind-turbine generator can reach efficiencies above 99 %.

Despite these advantages, the combination of IPM design with double-stator topologies has received little attention. Ibrahim et al. [26] introduced several double-stator generator variants using interior and embedded permanent magnets with S-, V-, and U-shaped rotor structures. Among these, the S-shaped Interior Embedded Double-Stator Generator (S-shaped IEDSG) demonstrated the lowest cogging torque and highest electrical output. This arrangement offers superior magnetic-flux utilization, reduced leakage, and increased power density features ideal for compact direct-drive renewable-energy generators [27].

While earlier studies analyzed the electromagnetic performance of the S-shaped IEDSG, its operation within a complete power-conversion and energy-storage system has not been explored. In particular, the coordinated operation of the generator with a Maximum Power Point Tracking (MPPT) controller and a Battery Management System (BMS) has not been experimentally validated. This study addresses that gap by integrating and experimentally validating the S-shaped IEDSG with an MPPT controller and BMS to assess system performance under different operating speeds. The analysis focuses on charging thresholds, current outputs, and charging durations for the inner, outer, and double-stator configurations. The findings also provide practical adoption insights, demonstrating that, compared with single-stator operation, the double-stator configuration enables earlier charging initiation, sustained high charging power, and shorter charging duration. These results establish the integrated S-shaped IEDSG as a practical and reliable solution for small-scale renewable energy systems such as pico-hydro and wind applications.

II. DESIGN, CONFIGURATION AND FABRICATION OF THE S-SHAPED IEDSG

A. STRUCTURAL DESIGN

Figure 1 illustrates the cross-sectional structure of the S-shaped Interior Embedded Double Stator Generator (S-shaped IEDSG), which consists of two stators, an outer stator and an inner stator, positioned on either side of a central rotor. Both stators are fixed and wound with copper coils that interact with the rotor's magnetic field to generate torque and electrical power. The rotor core is located between the stators and contains permanent magnets that establish the magnetic field required for energy conversion.

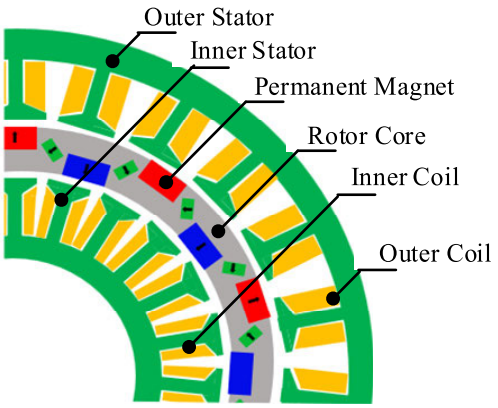

FIGURE 1. Quadrant Cross-sectional structure of S-shaped IEDSG.

The S-shaped permanent magnet configuration is a distinct design that incorporates elements of both embedded and internal permanent magnet arrangements. In an embedded permanent magnet design, only one surface of the magnet faces the inner or outer stator, whereas in an interior permanent magnet configuration, no surface of the magnet directly faces either stator.

The S-shaped permanent magnet design has a magnet arrangement that resembles the letter ''S'' when viewed from the side. This approach makes better use of magnetic material and has the potential to outperform typical interior and embedded permanent magnets.

For this magnetization direction setup, the interior of the rotor contains a single permanent magnet. This magnet's function is to increase the magnetic flux flow towards the

air gap and outer stator, hence improving the motor's performance. This segmentation prevents the magnetic flux from returning to the rotor without first travelling through the air gap and stator. By regulating the magnetic flux path, this design improves the generator's efficiency and overall performance.

Figure 3 demonstrates that magnetic flux is effectively guided through both the inner and outer stator air gaps. The inner stator reaches an average flux density of approximately 0.62 T, while the outer stator achieves about 0.70 T. The difference arises from their geometric parameters, as the inner stator accommodates fewer turns due to its smaller diameter. Despite this, the flux remains well distributed across both stators, indicating balanced utilization of the rotor's magnetic field. This confirms that each stator operates efficiently within its structural constraints, contributing to improved overall torque density and power performance of the machine.

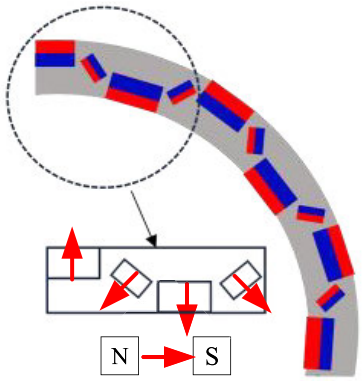

FIGURE 2. Quadrant magnetization direction of S-shaped IEDSG.

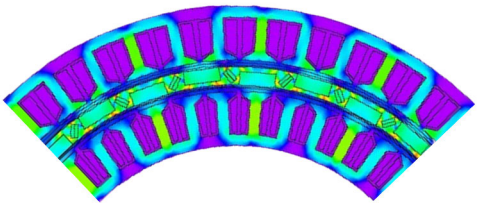

FIGURE 3. Flux density distribution of S-shaped IEDSG.

To evaluate the performance of the S-shaped IEDSG, both simulation and experimental testing are conducted using the design parameters summarized in Table 1. Key dimensions include the outer stator inner diameter of 300 mm, inner stator inner diameter of 176 mm, with a shared axial length of 30 mm. The generator is designed with 45 slots and 30 poles, providing a balance between torque production and electrical frequency. The air gap for both the inner and outer stator sides is set at 3 mm to ensure efficient magnetic flux interaction. High-performance NdFeB permanent magnets with dimensions of (15 × 6 × 30) mm and (3 × 6 × 30) mm are embedded and inserted in the rotor to enhance magnetic field strength. The stator and rotor cores are constructed using 50H800 steel to minimize core losses, while copper is used as the coil material to ensure high conductivity. These parameters are carefully selected to optimize power density, efficiency, and electromagnetic performance of the S-shaped IEDSG.

TABLE 1. Design parameter of IEDSG.

Design Parameter	Unit	Value
Outer Diameter	mm	300
Inner Diameter	mm	176
Axial Length	mm	30
Number of Slots	slot	45
Number of Poles	poles	30
Air Gap	mm	3
Interior PM	mm	3 × 6 × 30
Embedded PM	mm	15× 6 × 30
Inner-coil Turns	-	13
Outer-coil Turns	-	20
Permanent Magnet Material	-	NdFeB
Stator and Rotor Core Material	-	50H800
Coil Material	-	Copper

B. ELECTRICAL DESIGN CONFIGURATIONS

The two-dimensional finite element method (2D-FEM) analysis was performed using JMAG® software (JSOL Corporation) to evaluate the electromagnetic and electrical performance of the proposed S-shaped IEDSG. The electrical circuit configuration was modeled for both no-load and load conditions, including the effects of eddy currents. The generator output was connected to a three-phase full-wave diode rectifier (D1–D6) to enable DC-side performance evaluation.

The inner coil refers to the winding installed on the inner stator, while the outer coil corresponds to the winding installed on the outer stator. During experimental evaluation, the inner and outer coils were connected independently to the rectifier circuit to assess their individual electrical characteristics. The series-coil configuration refers to the electrical series connection of the inner and outer stator windings, allowing analysis of their combined output behavior.

Prior to series connection, the inner and outer stator windings were phase-matched to ensure consistent phase sequence and polarity. Phase alignment was verified experimentally under open-circuit conditions by comparing the induced phase voltages using a digital oscilloscope, confirming that the corresponding phase waveforms were in phase before series connection. This procedure prevents voltage cancellation and ensures constructive voltage addition in the series-connected double stator configuration.

In the no-load test setup, the rectifier was connected directly to the generator output with a no-load resistance applied across the DC terminals to evaluate magnetic behavior, including cogging and no-load torque characteristics. For load testing, a resistive load was connected across the

rectifier DC terminals, enabling measurement of output voltage, current, and power under various electrical loading and rotational speed conditions. The load resistance was adjusted systematically to characterize generator performance across different operating points.

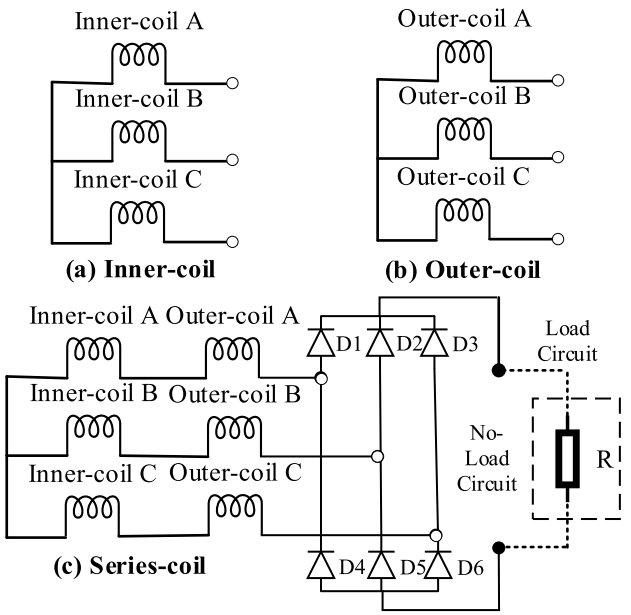

FIGURE 4. Electrical circuit configurations.

C. FABRICATION DESIGN

An S-shaped IEDSG is designed and built to compare results from simulation and experimental investigation. The final drawing of the S-shaped IEDSG is created with SolidWorks software. Figure 5(a) shows that the design is separated into six parts: the outer stator holder, the outer stator, the inner stator holder, the inner stator, the iron rotor core, and the iron rotor core holder. The inner stator, outer stator, iron rotor core, and permanent magnet have the same dimensions and design as those used in simulation. To ensure that the permanent magnet rotor rotates smoothly, the six sections are connected by bearing. Furthermore, the outer stator holder is locked to the inner stator holder, preventing the stator from moving. Figure 5(b) shows the completely built S-shaped IEDSG.

A detailed experimental examination is performed under both open-circuit and load circumstances, often known as the DC power test. The performance of the S-shaped IEDSG design is evaluated by measuring key electrical and mechanical characteristics such as generated voltage, current, output power, and electromagnetic torque. These metrics provide vital information about the generator's operational behaviour.

The preceding section described the structural configuration and integration of the S-shaped IEDSG with the MPPT controller and BMS, detailing the electrical and mechanical design parameters. To validate these design choices and assess the generator's electromagnetic behavior, experimental and simulation analyses were performed. The following section presents the testing methodology and corresponding results, including open-circuit voltage profiles, harmonic characteristics, and comparison of simulated and measured waveforms.

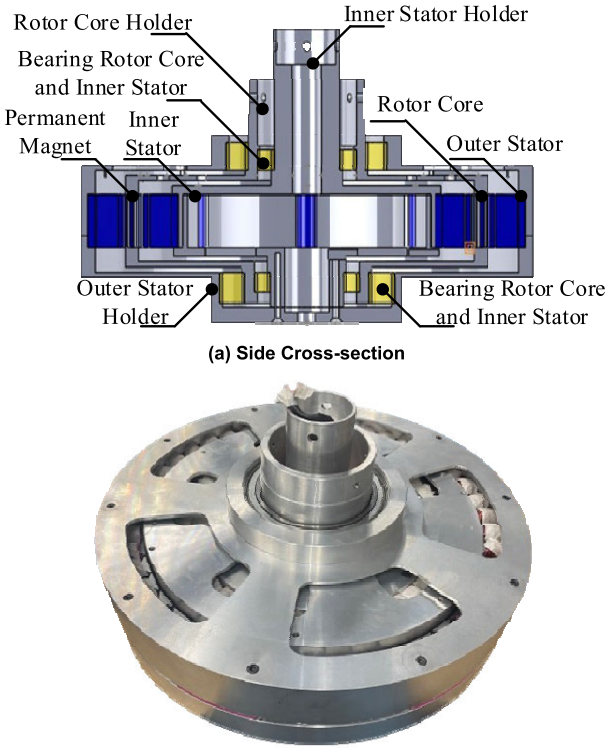

FIGURE 5. Fabricated S-shaped IEDSG.

III. EXPERIMENTAL ANALYSIS AND SIMULATION VALIDATION

A. EXPERIMENTAL CONFIGURATIONS

The open-circuit test is a primary examination used to determine the voltage production capability and waveform quality of the fabricated S-shaped IEDSG under no-load conditions. As shown in Figure 6(a), the generator is mechanically linked to a torque meter (Model: TRB-10k) and powered by a prime mover, a brushless DC (BLDC) motor (Model: HPM05KW-12-PZ) with a set rotational speed of 200 RPM. Although the torque sensor is capable of measuring both torque and rotational speed, in this study it was utilized solely to obtain accurate and stable speed data, directly representing the mechanical input to the generator. This controlled setup enables precise measurement of the induced voltages without the influence of load current.

The purpose of this test is to identify the greatest peak-to-peak voltage generated by S-shaped IEDSG and the sinusoidal features of the induced voltage. The S-shaped IEDSG's output terminals, which include inner-coil, outer-coil, and series-coil configurations, are each connected to a digital oscilloscope (Model: TDS2014B). Each of these coil sets represents a distinct phase winding, allowing for

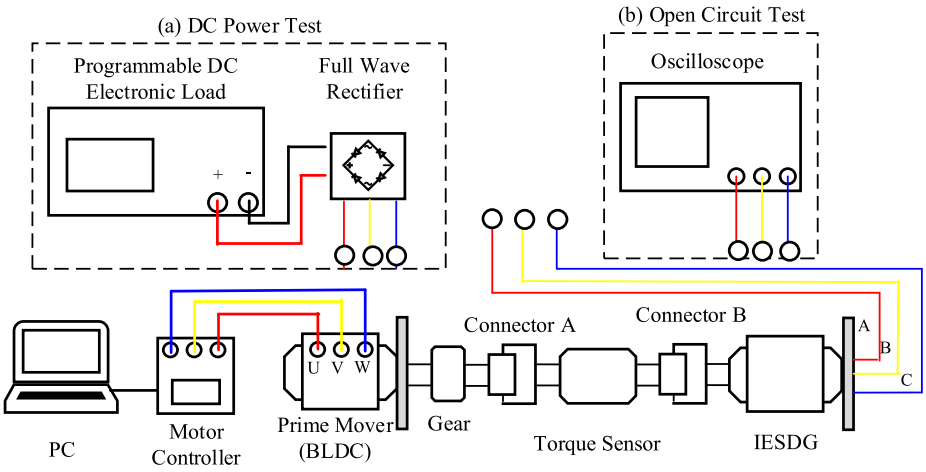

FIGURE 6. Open circuit and DC power measurement setup.

separate performance evaluations. When the BLDC motor drives the rotor, sinusoidal waveforms emerge on the oscilloscope, and the peak-to-peak voltages for each coil arrangement are recorded. This test provides critical insights into the electromagnetic design and coil arrangement of the IEDSG.

Figure 6(b) depicts the experimental setup utilised to assess the DC-side performance of the S-shaped IEDSG, namely its capacity to deliver usable power under resistive loading circumstances. In this test, the generator is linked to a motor controller (Model: HPC300-72300) that accurately controls the speed of the BLDC prime mover. The mechanical energy from the motor is conveyed through a magnetic gear assembly and a torque sensor before reaching the S-shaped IEDSG's rotor.

To convert the three-phase AC voltage generated by the generator into DC, the output is linked to a three-phase full-wave rectifier. A programmable electronic load is connected to the DC output of the full-wave rectifier to simulate various resistive load conditions. This system enables comprehensive testing across various electrical loading scenarios and rotational speeds. Each test point records key electrical metrics such as DC voltage, DC current, and DC power. These factors are critical in determining the power output capability of the S-shaped IEDSG.

B. OPEN CIRCUIT ANALYSIS

The open circuit test for fabricated S-shaped IEDSG evaluates its voltage characteristics under no load condition for series-coil and independent-coil including inner-coil and outer-coil winding. The single-phase voltage waveform is shown in Figure 7(a), where the voltage generated by the series-coil winding is higher compared to the outer-coil and inner-coil winding with the peak voltage of 30 V, indicating the additive of series connection. The outer-coil winding contributes moderately with the peak voltage of 25 V, while inner-coil winding generates the least voltage with the peak voltage of 10 V, due to fewer number of turns that affect a weaker magnetic flux leakage. The three-phase voltage waveform for series-coil connection is shown in Figure 7(b).

The frequency spectrum analysis of the measured AC voltage waveform, obtained through Fast Fourier Transform (FFT) as illustrated in Figure 8(a), clearly identifies a dominant fundamental component at 50 Hz, which corresponds to the generator's electrical frequency determined by the rotor speed and pole number. The harmonic spectrum in Figure 8(b) shows that the second harmonic at 100 Hz is the most significant distortion component, while higher-order harmonics (third to tenth) exhibit considerably lower magnitudes. The calculated Total Harmonic Distortion (THD) of approximately 25.2% indicates the presence of harmonic components superimposed on the fundamental waveform. This THD value refers to the open-circuit line voltage of the generator; after three-phase rectification and DC filtering, most of these harmonic components are suppressed, resulting in a minimal current ripple at the battery input. Consequently, the waveform quality remains acceptable for small-scale distributed generation and pico-hydro applications, where moderate distortion does not compromise operational stability. Following rectification, the DC output exhibits a substantially smoother voltage and current profile, confirming that the harmonic components observed in the open-circuit AC waveform have negligible influence on the charging behavior of the system.

C. DC POWER ANALYSIS

Figure 9(a) depicts the experimental results of electrical power generated by an S-shaped IEDSG, tested at rated speeds ranging from 200 RPM to 800 RPM. The electrical power output increases as the generator's rated speed increases. This trend suggests that increasing rotating speed improves flux linkage and electromotive force (EMF), resulting in a corresponding increase in power generation.

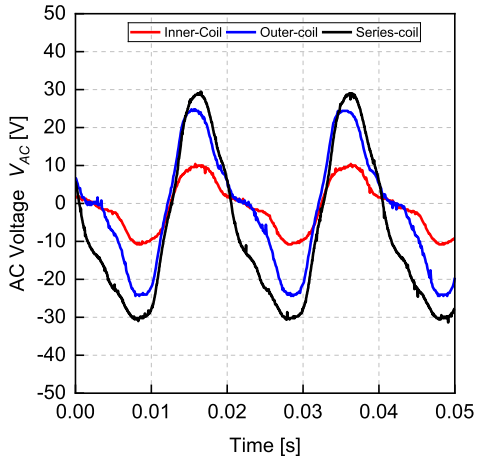

(a)Single Phase Voltage, comparing three coil configurations: Inner-coil, Outer-coil, and Series-coil

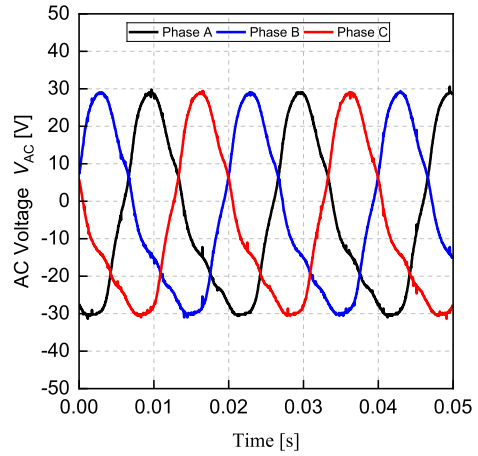

(b) Three Phase Voltage for the series-coil configuration

FIGURE 7. Open circuit test under no load conditions.

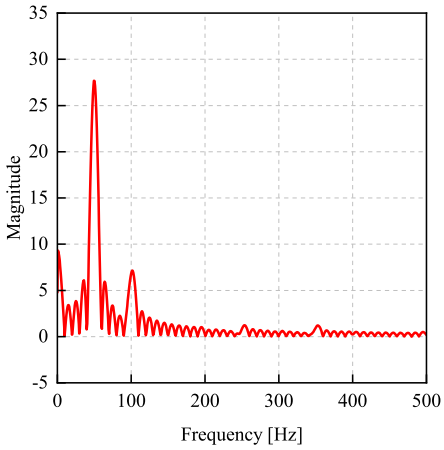

(a) FFT Spectrum of AC Voltage

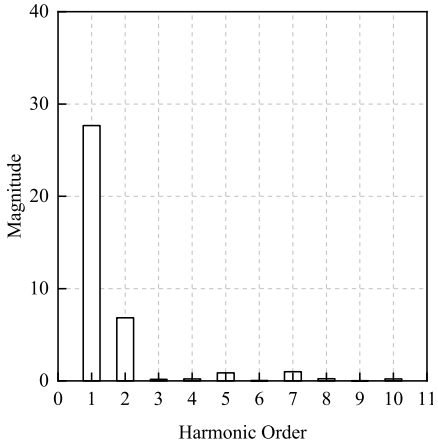

(b) Harmonic Spectrum of AC Voltage

FIGURE 8. Frequency spectrum analysis of AC voltage.

At 800 RPM, the generator produces the most electrical power, reaching 1247.71 W at peak performance.

For all rated speeds, the electrical power output rises quickly with load resistance in the early stages until peaking at a specified resistance value. After this point, the power begins to decrease as the load resistance increases. Peak power is achieved at around (4-10) ohm across all speed settings, after which the power output gradually drops as resistance increases. At 200 RPM, the power production is the lowest, peaking at approximately 210.27 W. As the speed doubles to 400 RPM, the power rises to around 507.04 W. At higher speeds (e.g., 600 RPM and 800 RPM), the power production peaks at 879.08 W and 1247.71 W, respectively. This scaling phenomenon reveals how power generation is directly related to rotational speed.

D. EXPERIMENTAL VALIDATION

Validating experimental and simulation results is crucial to ensuring that the simulation accurately portrays the generator's real-world behaviour. Both the experimental and simulation findings follow the same trend, indicating that the model adequately reflects generator behaviour at various load resistances. The differences observed are within an acceptable range, mainly due to inevitable variations between simulation assumptions and prototype fabrication. In simulation, the windings are considered perfectly distributed and the airgap ideally balanced, whereas in practice, manual coil placement and minor airgap unbalances occur, leading to small reductions in flux linkage and consequently lower measured voltage and power. The voltage gradually increases as the load resistance increases. This tendency happens because increasing resistance leads to decreased current, which reduces voltage drops caused by internal resistance. The percentage difference in electrical power between experiment and simulation at 200 rpm is approximately 14% at 2 ohm load resistance. The validation results demonstrate that the simulation model accurately represents the generator's experimental behaviour at 200 RPM.

The analysis in the previous section established strong agreement between the simulated and experimental results,

confirming the accuracy of the electromagnetic model and validating the S-shaped IEDSG design. Building upon these findings, the next section focuses on the integrated performance of the generator with the MPPT controller and BMS under practical operating conditions. This analysis examines charging voltage, current, and state-of-charge (SoC) behavior to evaluate the complete system performance and demonstrate the advantages of the double stator configuration.

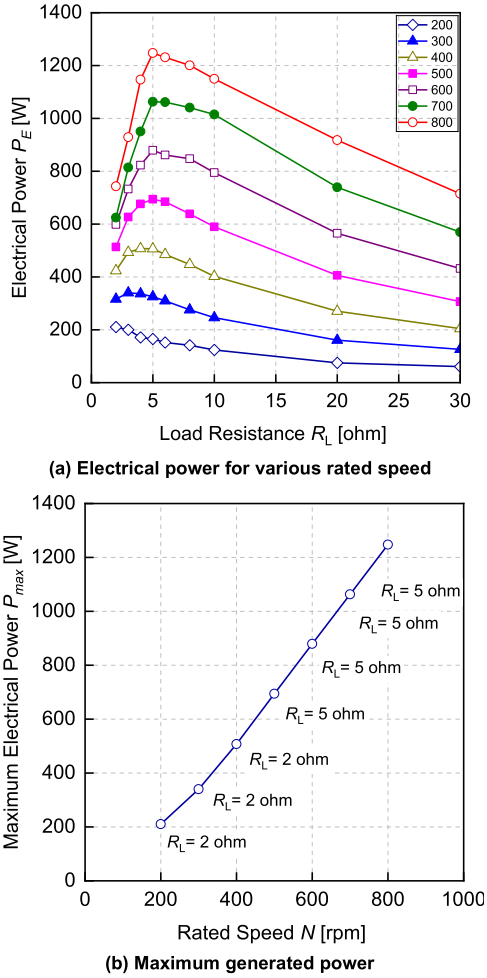

(a) Electrical power for various rated speed

(b) Maximum generated power

FIGURE 9. DC power test with various rated speed.

IV. INTEGRATED ANALYSIS OF S-SHAPED IEDSG WITH MPPT CONTROLLER AND BMS

This section presents the experimental validation that supports the main contributions of this study. A comparative investigation was carried out on the integrated S-shaped IEDSG with the MPPT controller and BMS to examine the differences in charging thresholds, current outputs, and charging durations among the inner-, outer-, and double-stator configurations under variable-speed conditions.

A. SYSTEM CONFIGURATIONS

To determine the real-world applicability of the proposed S-shaped IEDSG, an integrated experimental setup is created

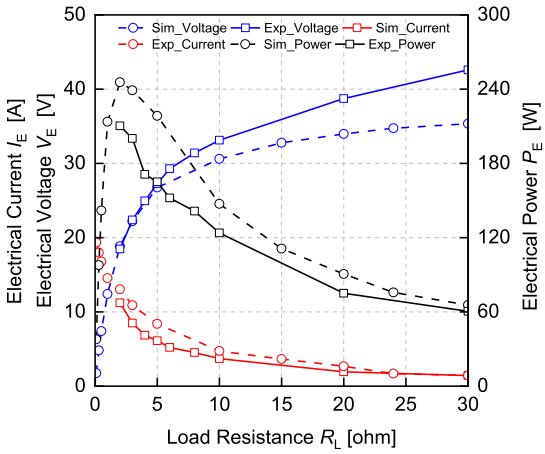

FIGURE 10. Validation Result of S-shaped IEDSG at 200 RPM.

that included the generator, MPPT controller, and BMS. This integration aims to optimize the energy harvesting process while also assuring safe and effective electrical energy storage.

The constructed S-shaped IEDSG is physically connected to a prime mover (DC motor) that is controlled by a programmable motor controller to ensure a constant rotational speed. A 72V power supply for the motor controller is provided by a battery pack consisting of six 12V lead acid batteries connected in series. This setup simulates a steady-state input source and enables consistent evaluation of the generator's performance under regulated operation conditions. The three-phase electrical output from the S-shaped IEDSG is routed to the MPPT controller, which dynamically adjusts the operating point to extract the most power from the generator under changing load conditions.

The MPPT controller is then connected to the BMS, which has two functions: it monitors vital battery parameters (such as cell voltage, current, and temperature) and protects the battery pack from circumstances that cause overcharging, over discharging, or thermal runaway. The BMS is linked to a battery bank made up of seven 3.2 V lithium-ion phosphate (LiFePO4) cells arranged to form a 24 V energy storage system.

To complement the experimental setup, a comprehensive electromagnetic–circuit simulation was performed using JMAG-Designer to emulate the integrated operation of the S-shaped IEDSG with the MPPT controller and BMS. In this simulation, the MPPT behavior was represented by estimating the effective load resistance corresponding to the maximum power point (MPP) for each stator configuration (inner, outer, and double). This equivalent resistance was applied in the generator's electrical circuit and systematically varied over a practical range to identify the optimal power operating region at each speed condition.

It should be emphasized that the equivalent MPPT resistance was introduced solely for simulation purposes to

represent the steady-state operating point achieved by the physically implemented MPPT controller during experimental charging. While the MPPT controller operates dynamically in the experimental system, the resistance-based representation enables efficient validation of generator performance without explicitly modeling the full MPPT control algorithm and battery dynamics. The integrated evaluation therefore focused on electrical and charging performance under controlled operating conditions; temperature rise and detailed copper and core loss separation were not investigated in this study.

This combined experimental and simulation approach provides a direct means of correlating simulation-based predictions with experimental measurements, ensuring consistency between both analyses and demonstrating the system's suitability for efficient energy harvesting and battery management in renewable energy applications.

The integration of the MPPT controller and BMS was validated to assess practical system performance. The design targets were to maximize power extraction across a variable input speed range, ensure reliable charging initiation once the DC bus voltage exceeded 22 V, and reduce the charging duration from 70 % to 100 % state of charge (SoC) to less than 400 minutes. These objectives were confirmed by the simulation and experimental results shown in Figures 12 and 13, where the system demonstrated stable operation and effective charging performance under different stator configurations.

This integrated configuration not only demonstrated the generator's capability to deliver stable power but also confirmed its compatibility with modern energy management and storage systems, reinforcing its suitability for distributed renewable energy applications such as pico-hydro and microgrid systems.

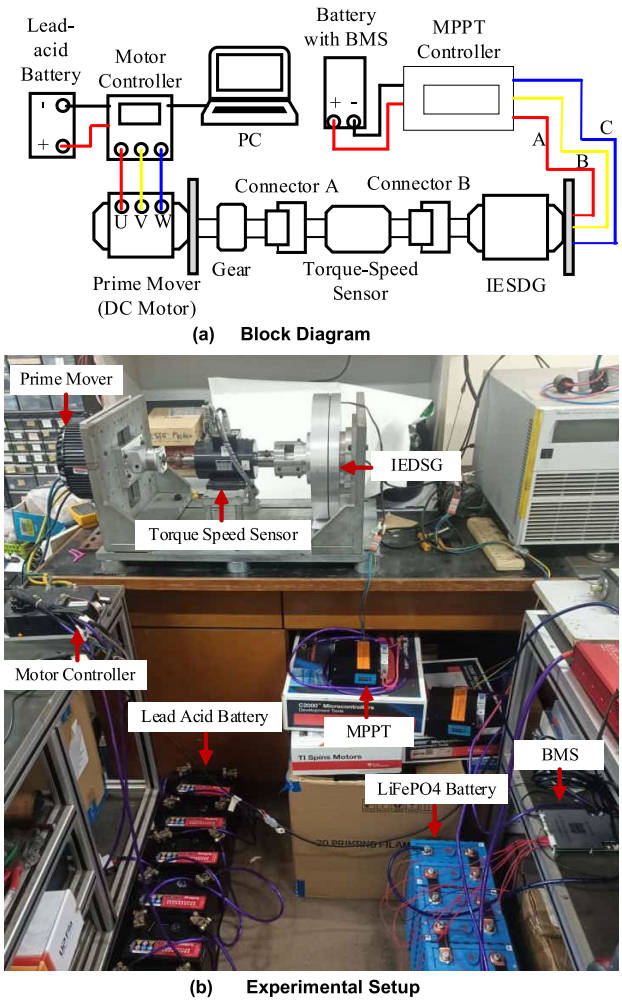

FIGURE 11. S-shaped IEDSG integrated with MPPT Controller and BMS system.

B. PERFORMANCE CHARACTERISTICS UNDER VARIABLE SPEEDS

Figure 12 presents the charging parameters of the S-shaped IEDSG integrated with the MPPT controller and BMS, including charging voltage, current, and power for the inner-, outer-, and double-stator configurations. Each subfigure ((a) to (c)) corresponds to one configuration and shows how the electrical characteristics vary with rotational speed.

A significant charging threshold occurs when the DC voltage exceeds 22 V, marking the transition from non-charging to active-charging mode. In the inner-stator configuration (Figure 12(a)), both experimental and simulation results show a gradual increase in voltage and current as speed increases. The charging process begins above 350 rpm, with power peaking at approximately 263 W experimentally and 237 W in simulation at 650 rpm. The percentage deviation between the two results is about 9.9 %, indicating strong agreement.

In the outer-stator configuration (Figure 12(b)), charging begins earlier around 150 rpm, but at lower current and power, reaching 183 W experimentally and 129 W in simulation. The double-stator configuration (Figure 12(c)) combines both stators in series, achieving early charging at the speed of 150 rpm while sustaining higher current and power, with 240 W experimentally and 260 W in simulation at 250 rpm.

The MPPT controller was physically implemented in the experimental setup and operated dynamically during charging. For simulation purposes, an equivalent MPPT load resistance was estimated via FEM analysis to represent the steady-state operating point achieved by the experimental MPPT controller at maximum power. This approach enables direct validation of simulation results against experimental measurements without explicitly modeling the full MPPT control algorithm.

The double-stator configuration exhibits the best correlation between the assumed resistance model and the experimental data, validating that the simulation approach can reliably predict the maximum-power operation under variable-speed conditions.

C. CHARGING CHARACTERISTICS

Figure 13 illustrates the comparative charging behavior of the S-shaped IEDSG system for the inner, outer, and double stator

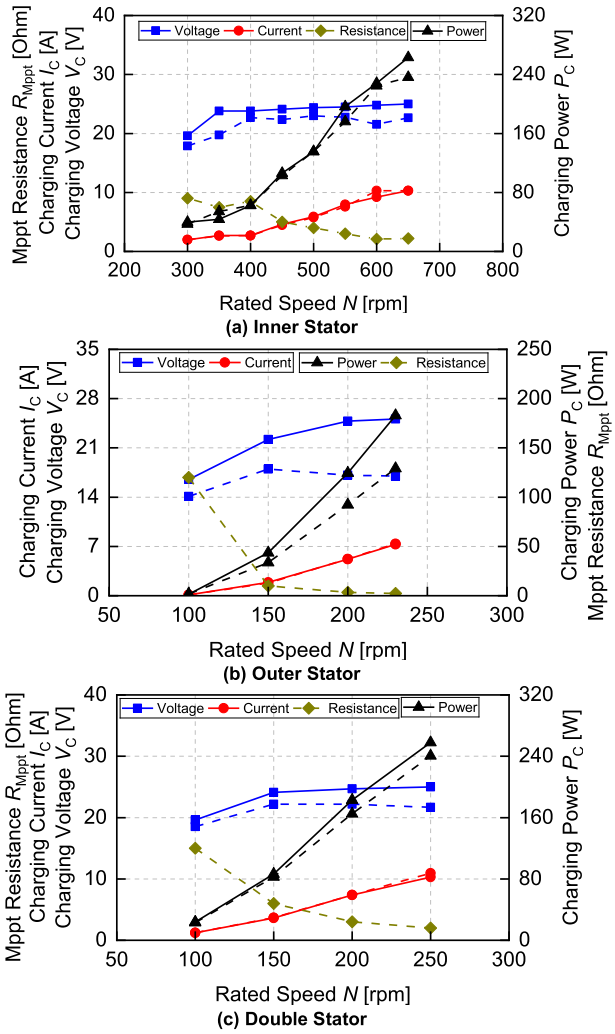

FIGURE 12. Charging characteristics under different stator configurations; Solid lines denote experimental results, dashed lines represent FEM-based simulation.

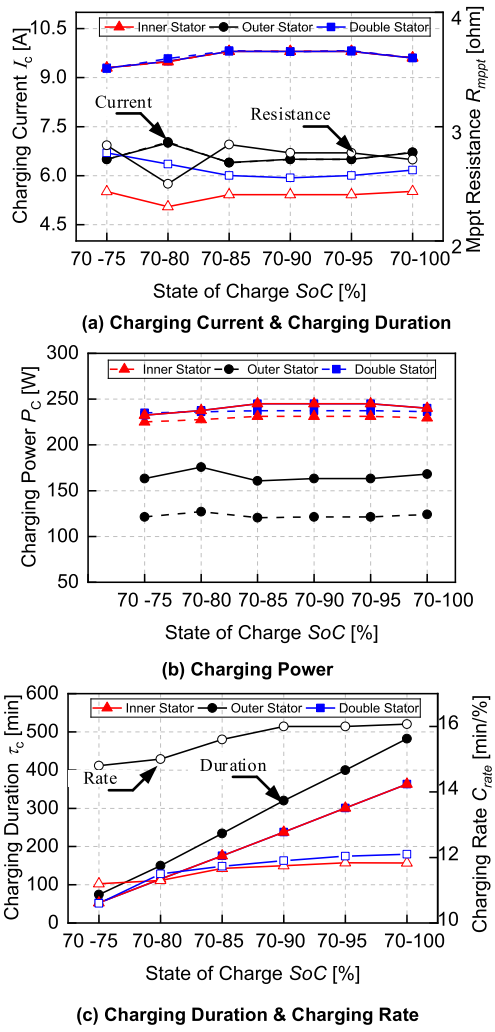

FIGURE 13. Battery Charging Behavior for Inner Stator (650 RPM), Outer Stator (230 RPM) and Double Stator (250 RPM); Solid lines denote experimental results, dashed lines represent FEM-based Simulation.

configurations within the 70 to 100 percent state of charge (SoC) range. Each configuration was tested at its respective optimum operating speed to represent realistic charging conditions: the inner stator at 650 revolutions per minute (rpm), the outer stator at 230 rpm, and the double stator at 250 rpm. These speeds correspond to the threshold required to generate approximately 25 volts, which marks the onset of active charging. The figure combines both experimental and simulation data to compare five main parameters: charging current, equivalent MPPT resistance, charging power, charging duration, and charging rate.

In Figure 13(a), the charging current and MPPT resistance are presented together. The double stator and inner stator configurations maintain the highest charging current levels, close to 10 amperes, across the SoC range. The inner stator achieves this performance because it operates at a higher speed of 650 rpm, which enhances magnetic flux flow and raises the output voltage to about 25 volts. The outer stator, running at 230 rpm, generates lower current due to weaker magnetic coupling and reduced flux linkage. The MPPT resistance follows an inverse trend, where the double stator exhibits the lowest equivalent resistance, indicating more effective power transfer and higher conversion efficiency. The combined action of both stators in the double stator configuration strengthens magnetic flux coupling even at lower rotational speed, improving the overall energy transfer capability.

Figure 13(b) compares the charging power for the three configurations. The double stator consistently delivers the highest charging power, ranging from 240 to 250 watts, followed by the inner stator at about 230 watts. The outer stator remains below 200 watts throughout the SoC range. This clearly demonstrates that coupling both stators enhances power delivery and provides more stable charging performance under varying operating conditions.

Figure 13(c) shows the relationship between charging duration and charging rate from 70 to 100 percent SoC.

Both the double stator and inner stator configurations achieve full charge in less than 400 minutes, while the outer stator requires more than 500 minutes. The double stator also exhibits the highest charging rate, indicating superior energy transfer efficiency. Although the charging performance of the inner and double stator configurations appears similar in terms of duration and rate, the inner stator achieves this result only at a higher rotational speed of 650 rpm. In contrast, the double stator attains comparable performance at a much lower speed of 250 rpm, confirming its advantage in accelerating the charging process while maintaining high energy conversion efficiency under low-speed operation.

Overall, the results confirm that the double stator configuration offers the most balanced and efficient performance by combining high current, low MPPT resistance, high charging power, and shorter charging duration. The strong agreement between the experimental and simulation results validates the FEM-based MPPT resistance estimation and demonstrates that the integrated S-shaped IEDSG with the MPPT controller and BMS delivers stable, efficient, and low-speed-compatible charging performance suitable for compact renewable energy systems such as pico-hydro and small-scale wind generators.

From a comparative perspective, the three stator configurations exhibit distinct and quantifiable performance trade-offs when evaluated using the same charging criteria. The inner stator configuration provides the highest peak charging power but requires a substantially higher rotational speed to initiate and sustain charging, limiting its applicability in low-speed renewable environments. The outer stator configuration enables early charging at low speed but suffers from reduced current capability and extended charging duration. By contrast, the double stator configuration effectively combines the advantages of both single-stator modes, achieving early charging initiation, maintaining high charging power, and significantly reducing charging time at a much lower operating speed. This experimental comparison confirms that the double stator configuration offers the most balanced and application-relevant performance among the three configurations.

V. CONCLUSION

This paper presented the integration and experimental validation of an S-shaped Interior Embedded Double Stator Generator (S-shaped IEDSG) combined with a Maximum Power Point Tracking (MPPT) controller and a Battery Management System (BMS) for renewable energy applications. The system was developed to provide stable power extraction and safe battery charging under different operating speeds. Comparative experiments were conducted for three stator configurations, inner stator, outer stator, and double stator, to examine their charging thresholds, current outputs, and charging durations. The inner stator produced the highest peak charging power of 263 W but required higher rotational speed of 650 rpm to initiate charging. The outer stator began charging earlier at 150 rpm but showed lower current and longer charging time exceeding 500 minutes. The double stator configuration provided the most balanced performance by achieving early charging initiation, maintaining high charging power of approximately 250 W, and completing charging in less than 400 minutes when charging from 70 % to 100 % state of charge. These results confirm that the double stator design provides a practical improvement over single stator arrangements, enabling faster and more stable charging while maintaining compactness and simplicity. The integrated S-shaped IEDSG with the MPPT and BMS demonstrates strong potential for small-scale renewable energy systems such as pico-hydro and wind generation, where low speed operation, reliability, and continuous energy storage are required.

REFERENCES

[1] F. Wu, X.-P. Zhang, and P. Ju, "Small signal stability analysis and control of the wind turbine with the direct-drive permanent magnet generator integrated to the grid," *Electric Power Syst. Res.*, vol. 79, no. 12, pp. 1661–1667, Dec. 2009.

[2] Y. Chen, Z. Wang, and S. Yonghuan, "The simulation of direct drive square-wave permanent magnet synchronous wind generator control system," *J. Syst. Simul.*, vol. 21, pp. 5849–5855, Sep. 2009.

[3] M. L. Rahman, S. Oka, and Y. Shirai, "Hybrid power generation system using offshore-wind turbine and tidal turbine for power fluctuation compensation (HOT-PC)," *IEEE Trans. Sustain. Energy*, vol. 1, no. 2, pp. 92–98, Jul. 2010.

[4] Y. Yasa and E. Mese, "Design and analysis of generator and converters for outer rotor direct drive gearless small-scale wind turbines," in *Proc. Renew. Energy Res. Appl. (ICRERA)*, 2014, pp. 1–12.

[5] P. Zheng, Q. Wu, J. Bai, C. Tong, and Z. Song, "Analysis and experiment of a novel brushless double rotor machine for power-split hybrid electrical vehicle applications," *Energies*, vol. 6, no. 7, pp. 3209–3223, Jul. 2013.

[6] C. A. Vaithilingam, N. Misron, M. R. Zare, I. Aris, and M. H. Marhaban, "Computation of electromagnetic torque in a double rotor switched reluctance motor using flux tube methods," *Energies*, vol. 5, no. 10, pp. 4008–4026, Oct. 2012.

[7] J. F. Gieras, R.-J. Wang, and M. J. Kamper, *Axial Flux Permanent Magnet Brushless Machines*. Dordrecht, The Netherlands: Kluwer Academic, 2004.

[8] J. R. Hendershot and T. J. E. Miller, *Design of Brushless Permanent-Magnet Machines*. U.K.: Motor Design Books, 2010.

[9] F. Chai, S. Cui, and S. Cheng, "Performance analysis of double stator starter generator for the hybrid electric vehicle," *IEEE Trans. Magn.*, vol. 41, no. 1, pp. 484–487, Jan. 2005.

[10] K. T. Chau, Y. B. Li, J. Z. Jiang, and C. Liu, "Design and analysis of a stator-doubly-fed doubly-salient permanent-magnet machine for automotive engines," *IEEE Trans. Magn.*, vol. 42, no. 10, pp. 3470–3472, Oct. 2006.

[11] C. Liu, K. T. Chau, J. Z. Jiang, and L. Jian, "Design of a new outer-rotor permanent magnet hybrid machine for wind power generation," *IEEE Trans. Magn.*, vol. 44, no. 6, pp. 1494–1497, Jun. 2008.

[12] M. Norhisam, M. Norafiza, and C. Y. Sia, "Double stator type permanent magnet generator," in *Proc. IEEE Student Conf. Res. Develop. (SCOReD)*, Nov. 2009, pp. 316–319.

[13] Y. Wang, S. Niu, and W. Fu, "Electromagnetic performance analysis of novel flux-regulatable permanent magnet machines for wide constant-power speed range operation," *Energies*, vol. 8, no. 12, pp. 13971–13984, Dec. 2015.

[14] M. Norhisam, S. Ridzuan, R. N. Firdaus, C. V. Aravind, H. Wakiwaka, and M. Nirei, "Comparative evaluation on power-speed density of portable permanent magnet generators for agricultural application," *Prog. Electromagn. Res.*, vol. 129, pp. 345–363, 2012.

[15] M. Norhisam, M. Nirei, M. Norafiza, C. Y. Sia, and H. Wakiwaka, "Basic characteristics of double stator slot-type permanent magnet generator," *J. Magn. Soc. Jpn.*, vol. 34, no. 3, pp. 385–388, 2010.

[16] S. Yang, F. Zhang, Z. Zhang, and H. Liu, "Design of double stator permanent magnet synchronous motor with low speed large torque," *IEEE Trans. Ind. Appl.*, 2018.

[17] Z. Wang, B. Liu, L. Guan, Y. Zhang, M. Cheng, B. Zhang, and L. Xu, "A dual-channel magnetically integrated EV chargers based on double-stator-winding permanent-magnet synchronous machines," *IEEE Trans. Ind. Appl.*, vol. 55, no. 2, pp. 1941–1953, Mar. 2019.
[18] W. Gul, Q. Gao, and W. Lenwari, "Optimal design of a 5-MW double-stator single-rotor PMSG for offshore direct drive wind turbines," *IEEE Trans. Ind. Appl.*, vol. 56, no. 1, pp. 216–225, Jan. 2020.
[19] A. Flah, I. A. Khan, A. Agarwal, L. Sbita, and M. G. Simoes, "Field-oriented control strategy for double-stator single-rotor and double-rotor single-stator permanent magnet machine: Design and operation," *Comput. Electr. Eng.*, vol. 90, Mar. 2021, Art. no. 106953.
[20] L. Yu, Z. Zhang, Z. Chen, and Y. Yan, "Analysis and verification of the doubly salient brushless DC generator for automobile auxiliary power unit application," *IEEE Trans. Ind. Electron.*, vol. 61, no. 12, pp. 6655–6663, Dec. 2014.
[21] D.-K. Hong, W. Hwang, J.-Y. Lee, and B.-C. Woo, "Design, analysis, and experimental validation of a permanent magnet synchronous motor for articulated robot applications," *IEEE Trans. Magn.*, vol. 54, no. 3, pp. 1–4, Mar. 2018.
[22] I. Safdar, S. Sultan, H. A. Raza, M. Umer, and M. Ali, "Empirical analysis of turbine and generator efficiency of a pico hydro system," *Sustain. Energy Technol. Assessments*, vol. 37, pp. 1–7, Feb. 2020.
[23] Z. Alnasir and M. Kazerani, "An analytical literature review of stand-alone wind energy conversion systems from generator viewpoint," *Renew. Sustain. Energy Rev.*, vol. 28, pp. 1–19, Dec. 2013.
[24] H. Chen, R. Qu, J. Li, and B. Zhao, "Comparison of interior and surface permanent magnet machines with fractional slot concentrated windings for direct-drive wind generators," in *Proc. 17th Int. Conf. Electr. Mach. Syst. (ICEMS)*, Hangzhou, China, Oct. 2014, pp. 2612–2617.
[25] P. Roshanfekr, T. Thiringer, M. Alatalo, and S. Lundmark, "Performance of two 5 MW permanent magnet wind turbine generators using surface mounted and interior mounted magnets," in *Proc. XXth Int. Conf. Electr. Mach.*, Marseille, France, Sep. 2012, pp. 1041–1047.
[26] N. Ibrahim, N. Misron, C. A. Vaithilingam, I. Aris, and N. F. Mailah, "Performance analysis of interior and embedded permanent magnet for double stator generator," *J. Eng. Sci. Technol.*, pp. 33–42, 2022.
[27] N. A. Ibrahim, N. Misron, C. A. Vaithilingam, I. Aris, and N. F. Mailah, "Basic characteristics of interior and embedded permanent magnet for double stator generator," *J. Eng. Sci. Technol.*, pp. 1–12, 2022.
[28] O. Zamzoum, Y. El, M. Errouha, A. Derouich, and A. El, "Active and reactive power control of wind turbine based on doubly fed induction generator using adaptive sliding mode approach," *Int. J. Adv. Comput. Sci. Appl.*, vol. 10, no. 2, 2019.

NUR AMIRA IBRAHIM was born in Klang, Selangor, Malaysia. She received the Bachelor of Engineering degree in electrical and electronics from Universiti Putra Malaysia, Malaysia, in 2020. She is currently pursuing the Ph.D. degree with the Faculty of Engineering. Her current research interest includes the development of permanent magnet synchronous generator for renewable energy applications.

NORHISAM MISRON (Member, IEEE) received the B.Eng., M.Eng., and Dr.Eng. degrees in system engineering from Shinshu University, Nagano, Japan, in 1998, 2000, and 2003, respectively. He joined as a Lecturer with the Department of Electrical and Electronic Engineering, Universiti Putra Malaysia, in 2003, advancing to an Associate Professor, in 2009, and a Full Professor, in 2016. He is currently an Associate Researcher with the Institute of Advanced Technology (ITMA) and the Institute of Plantation Studies (IPS). His current work focuses on designing and developing sensor and actuator technologies for the oil palm industry as well as motors and generators for clean energy. His research interests encompass magnetic applications, particularly in sensor, and electrical machine development. He actively serves on various IEEE technical committees.

HAIRUL FAIZI HAIRULNIZAM was born in Seremban, Negeri Sembilan, Malaysia. He received the bachelor's degree in electrical and electronics engineering from Universiti Putra Malaysia, in 2023. He is currently pursuing the master's degree, which he dedicated to innovating permanent magnet synchronous motor technology. His research interests include enhancing motor performance and application versatility.

ADAM ADZRIN SYAH was born in Negeri Sembilan, Malaysia. He received the bachelor's degree in electrical and electronics engineering from Universiti Putra Malaysia, in 2024.

CHOCKALINGAM ARAVIND VAITHILINGAM (Senior Member, IEEE) received the Ph.D. degree, in 2013. He is currently the Director of the Clean Technology Impact Laboratory, Taylor's University, Malaysia. His research work is aligned with the sustainable developmental goals on clean water sanitation (SDG6) and affordable and clean energy (SDG7).